Arabian Journal of Chemistry (2020) 13, 7490–7503

King Saud University

Arabian Journal of Chemistry

www.ksu.edu.sa
www.sciencedirect.com

ORIGINAL ARTICLE

Noble metallic nanoparticles from waste *Nypa fruticans* fruit husk: Biosynthesis, characterization, antibacterial activity and recyclable catalysis

Van-Dat Doan [a], Minh-Tan Phung [a,b], Thi Lan-Huong Nguyen [c], Thanh-Chi Mai [d], Thanh-Danh Nguyen [b,d,*]

[a] *Faculty of Chemical Engineering, Industrial University of Ho Chi Minh City, Ho Chi Minh City, Viet Nam*
[b] *Institute of Research and Development, Duy Tan University, Da Nang City, Viet Nam*
[c] *Institute of Biotechnology and Food Technology, Industrial University of Ho Chi Minh City, Ho Chi Minh City, Viet Nam*
[d] *Institute of Chemical Technology, Vietnam Academy of Science and Technology, 1 Mac Dinh Chi Street, District 1, Ho Chi Minh City, Vietnam*

Received 2 July 2020; accepted 22 August 2020
Available online 29 August 2020

KEYWORDS

Nypa fruticans fruit husk;
Waste;
Reduction;
Nitrophenol;
Antibacterial;
Recyclable catalysis

Abstract Biogenic synthesis of noble metal nanoparticles is particularly interested due to the effective applications for plasmonic catalysis and bioactivity. In this work, aqueous extract of waste *Nypa fruticans* (NF) fruit husk was utilized to synthesize silver nanoparticles (NF-AgNPs) and gold nanoparticles (NF-AuNPs). The effected parameters on the green reduction of metallic nanoparticles (MNPs) were investigated. Under optimum conditions of concentration, temperature and time, the biosynthesized NF-AgNPs and NF-AuNPs showed spherical nanoparticles with average size of 10–15 nm and 15–20 nm, respectively. The presence of AgCl in NF-AgNPs has been demonstrated by X-ray diffraction analysis. The elemental components of all samples confirmed the presence of anions and cations come from the aqueous extract. The biosynthesized nanoparticles were evaluated bacterial activity against three bacterial strains. NF-AgNPs exhibited selective antibacterial activity against *Bacillus cereus* but no activity against *Staphylococcus aureus* and *Salmonella typhimurium* at all tested concentrations. The recyclable catalysis activity of the biosynthesized nanoparticles was evaluated for the reduction of nitrophenols in the presence of sodium borohydride which possessed good catalytic performance in six running numbers. Additionally, AgCl played role as a source supplying AgNPs has been demonstrated in catalytic reduction of *p*-nitrophenol. For study

* Corresponding author at: Institute of Chemical Technology, Vietnam Academy of Science and Technology, 1 Mac Dinh Chi Street, District 1, Ho Chi Minh City, Vietnam.
E-mail addresses: danh5463bd@yahoo.com, nguyenthanhdanh3@duytan.edu.vn (T.-D. Nguyen).
Peer review under responsibility of King Saud University.

Production and hosting by Elsevier

https://doi.org/10.1016/j.arabjc.2020.08.024

of catalytic kinetic, NF-AgNPs possessed higher rate constant in comparison with NF-AuNPs whereas TOF values of NF-AuNPs was determined to be higher than those of NF-AgNPs.

1. Introduction

Metallic nanoparticles (MNPs) have found many applications in various fields such as optics, medicine, biology, catalysis and water treatment (Ly and Joo, 2020; Nam, et al. 2020; Darabdhara et al. 2019; Nguyen et al., 2018a,b; Hui et al. 2019; Khan et al. 2020). Amongst them, silver and gold nanoparticles have been particularly considered due to their excellent biocompatibility, physicochemical properties and catalytic efficiency. On the other hand, green synthesis of MNPs has paid increasing attention over chemical and physical methods. The green approaches using bio-sources such as fungi, bacteria and plants possess many advantages such as eco-friendliness, low-cost, availability and simple technique (Vetchinkina et al. 2019; Abdelghany et al. 2018; Kalantari et al. 2019; Jamila et al., 2020). During the past decades, the biosynthesis of MNPs using plant extract has been an important topic in nanotechnology due to improvement in bioactivity, human health and environmental issues (Burlacu et al. 2019; Nasrollahzadeh et al. 2019; Sharma et al. 2019; Das et al. 2018). It is approved that bioactive molecules with water-soluble polyol components are responsible in reduction and stabilization of biogenic MNPs. In recent years, the biogenic AgNPs and AuNPs with high antimicrobial activity have been important materials widely applied for agricultural and pharmaceutical fields (Rafique et al. 2017). Most of the studies on the biosynthesis of MNPs use the fresh plant as a reducing source. However, the use of waste source gains considerable economic benefits. Several recent reports have utilized effectively waste parts generated from agricultural sources which contain the high contents of secondary metabolites responsible for synthesis of MNPs (Vishwasrao et al. 2019; Dodevska et al. 2019; Agnihotri et al. 2018; Song et al. 2019).

On the other hand, the biogenic MNPs are well known to be effective catalysts for the complete degradation of toxic effluents and hydrogenation of nitroaromatic compounds (Singhal and Gupta, 2018; Ghasemi et al. 2020; Vinay et al. 2020; Khan et al. 2017; Francis et al. 2017). The later reaction is an important key in organic chemistry and pharmaceutical applications. Amino-based derivatives which are enormously used as a potent intermediate for manufacturing of many drugs have been synthesized from hydrogenation of nitro group (Zhu et al. 2019). However, very few reports on recyclability of the biogenic MNPs used as a heterogeneous catalyst in aqueous medium have been carried out (Veisi et al. 2018; Wang et al. 2019).

Nypa fruticans, Nipa palm is a monoecious palm that grows in river estuary and brackish water. Nipa palm thrives abundantly in Ryukyu Islands, southward to north Queensland and Southeast Asia (Uhl 1972). In Vietnam, Nipa palm is planted popularly to curb coastal erosion in Mekong Delta (Fagherazzi et al. 2017). Nowadays, various use of its production contributes to develop agricultural field in coastal communities. For instants, the sap containing 14–17% sucrose is utilized to manufacture vinegar, toddy or sugar and the fruit is used as local desserts or made into alcoholic beverages (Hamilton and Murphy 1988; Phetrit et al. 2020). As a result, abundant amount of the fruit husk is eliminated to the environment as a waste source. The major chemical components of fruit husk have been determined to include inorganic compounds, cellulose, hemicellulose, lignin, protein and others (Tamunaidu and Saka, 2011). In this study, we used aqueous extract of waste Nipa palm fruit husk as reducing and stabilizing agents for biosynthesis of AgNPs and AuNPs. The optimized nanoparticles were well characterized by analytic techniques and applied as antibacterial agents and recyclable catalysts for reduction of *o-, m-, p*-nitrophenols.

2. Experimental

2.1. Materials

All chemicals for synthesis were purchased from Acros (Belgium) in analytical grade and used without further purification. Distilled water was used throughout. The *Nypa fruticans* fruit husk was collected in HoChiMinh City, Vietnam.

2.2. Preparation of Nypa fruticans fruit husk extract

The NF fruit husk was washed completely with distilled water to remove any medium components and dried in an oven during 48 h at 80 °C. The dried powder of NF fruit husk was obtained after grounding process using an electronic blender. The dried powder (10 g) was refluxed with 100 mL of the water for 2 h. The aqueous solution was filtered under reduced pressure and added with water to obtain 100 mL of solution. The extract was stored at 4 °C in the refrigerator. The resultant solution was used as reducing and capping agents for biosynthesis of metallic nanoparticles. The crude solid obtained from concentrated process of the extract in a rotary vacuum was used for relating characterizations of the extract.

2.3. Biosynthesis and optimization of nanoparticles

In a typical procedure for the biosynthesis of noble MNPs, filtrate of NF extract (1 mL) was mixed with aqueous solution of metallic ions under vigorous stirring in dark. In all experiments, the volume of NF extract (1 mL) was kept constant. The formation of nanoparticles was associated with changes in colors of the solutions. After completing reaction, the biosynthesized nanoparticles were centrifuged at 10,000 rpm for 30 min and washed thrice with distilled water. The samples were dried in the oven for 24 h. The optimization process was carried out toward the best morphology and size of nanoparticles. The effect of principle parameters including metallic ion concentration, reaction temperature and reaction time was investigated to reach optimum condition of the biosynthe-

sis. For optimization process, UV–vis method scanned in range of 300–700 nm was used to recognize changes in nanoparticles concentration and morphology. The absorbance of NF-AgNPs and NF-AuNPs was measured in ranges of 400–435 nm and 520–540 nm, respectively.

2.4. Characterization of nanoparticles

Fourier transform infrared (FT-IR, Bruker, Tensor 27, Germany) was registered with the wavelength ranging from 500 to 4000 cm^{-1}. Morphology and size of the biosynthesized MNPs were determined by microscopy such as scanning electron microscopy (SEM, S-4800 HI-9057-0006) and transmission electron microscopy (TEM, JEOL JEM-1400). The crystallinity of MNPs was determined by various techniques including powder X-ray diffraction (XRD, 6100 X-ray diffractometer Shimadzu, Japan) and high resolution transmission electron microscopy (HRTEM, Tecnai G2 20 S-TWIN, FEI set at 200 kV) with measuring selected area electron diffraction (SAED) patterns. An analyzer Horiba (EMAX Energy EX-400) was used to analyze energy dispersive X-ray spectroscopy (EDX) of the powder nanoparticles.

2.5. Antibacterial activity of nanoparticles

The antibacterial activity of the biosynthesized MNPs was tested against two Gram-positive bacterial strains (*Bacillus cereus, Staphylococcus aureus*) and Gram-negative bacterial strain (*Salmonella typhimurium*) by the disk diffusion method. Briefly, each aliquot (50 µL) was added to 6 mm-diameter paper disks. Mueller Hinton agar was served as medium for the bacterial growth which was taken in the Petri plates with bacterial culture of brain-heart infusion (100 µL, 10^6 CFU/mL). The tested samples were prepared by dissolving the nanoparticle solutions to the required concentrations. The NF-AgNPs solutions were diluted at various concentrations of 0.62, 1.24, 2.48 and 4.96 µg/mL and The NF-AuNPs solutions were diluted at various concentrations of 1.12, 2.24, 4.48, and 8.96 µg/mL. The agar plates were incubated at 37 °C/24 h. The antibacterial activity of synthesized nanoparticles was evaluated by the zone of incubation around the well.

2.6. Catalytic activity of nanoparticles

The performance of NF-AgNPs and NF-AuNPs was investigated toward the catalytic reduction of nitrophenols including *o*-, *m*-, *p*-nitrophenol at the room temperature. An excess amount of $NaBH_4$ was used as a reducing reagent. For the reduction, 2.5 mL of each nitrophenol (0.1 mM) and 0.5 mL of $NaBH_4$ solution (0.1 M) were put into the cuvette and recorded its spectrum. Then 3 mg of catalysts were added to the reaction mixture. Performance of the reduction was determined by UV–Vis measurements. A rapid decrease of absorbance at the corresponding peaks could be observed for the respective nitrophenols. For study of kinetics, because the concentration of $NaBH_4$ used was much greater than concentration of nitrophenols, it was expected that the reduction would proceed according to the pseudo-first-order reaction. Thus, kinetics of the reduction can be described by the equation $\ln(A_t/A_0) = -kt$, where k is the reaction rate constant (s^{-1}) which can be found from slope of the straight line generated by plots of $\ln(A_t/A_0)$ versus the reaction time, t is the reaction time (s), A_0 and A_t are the amount of nitrophenol absorbance at time zero and t, respectively. For the reusability of catalysts, the nanoparticles were washed with distilled water and ethanol several times before reused.

3. Results and discussion

3.1. Biosynthesis of the nanoparticles

Biomolecules such as phenolics and proteins contained in the extract play a principle role in reducing metallic ions and stabilizing nanoparticles. In mechanism of this reduction, unstable phenoxyl radicals formed from the oxidation of phenolic groups consistently reduce the metallic ions and the metal nuclei produced from flocculation (Mosaviniya et al. 2019). The biosynthetic process and structure of MNPs are also well known significant dependence on the ionic components presented in the plant extract (Doan et al. 2020). These compositions can be included in nanoparticles product which can induce changes in their property and activity. Thus, ionic contents in the extract should be investigated before the fabrication of MNPs. In this study, content of anions including Cl^-, Br^-, NO_3^-, SO_4^{2-}, PO_4^{3-} is determined by ion chromatography technique while content of cations Na^+, K^+, Mg^{2+}, Ca^{2+} is determined by ICP-MS technique. Results are shown in Fig. 1. The concentration of Cl^- (79 mM) is very much higher than concentration of the others. In comparison with the corn-cob extract reported previously, content of ion Cl^- presented in NF fruit husk extract is double while content of anions NO_3^-, SO_4^{2-}, PO_4^{3-} is significantly lower (Doan et al. 2020). Dominance of chloride ions in the aqueous solution can form crystalline chloride salt of metallic ions such as Ag^+ during formation process of the biosynthesized nanoparticles. For investigation of cations, concentration of ion Ca^{2+} presented in the extract is not very significant while the other ions possess high concentrations in order of K^+ (83 mM), Na^+ (39 mM), Mg^{2+} (6 mM). The presence of the inorganic components in the aqueous extract is supported by the powder EDX analysis of NF fruit husk as reported previously (Tamunaidu and Saka, 2011).

The route for biogenic synthesis of AgNPs and AuNPs is illustrated in Fig. 2. The fruit husk was treated to remove unwanted components before refluxed with distilled water to obtain yellow NF extract. The extract is utilized to reduce metallic ions and stabilize nanoparticles. The formation of MNPs can be confirmed by relating color changes. The differ-

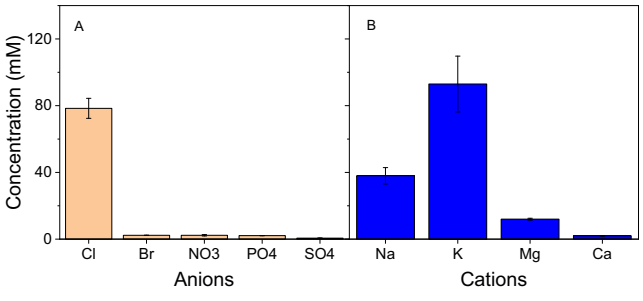

Fig. 1 Content of anions (A) and cations (B) presented in the aqueous extract of waste *Nypa fruticans* fruit husk.

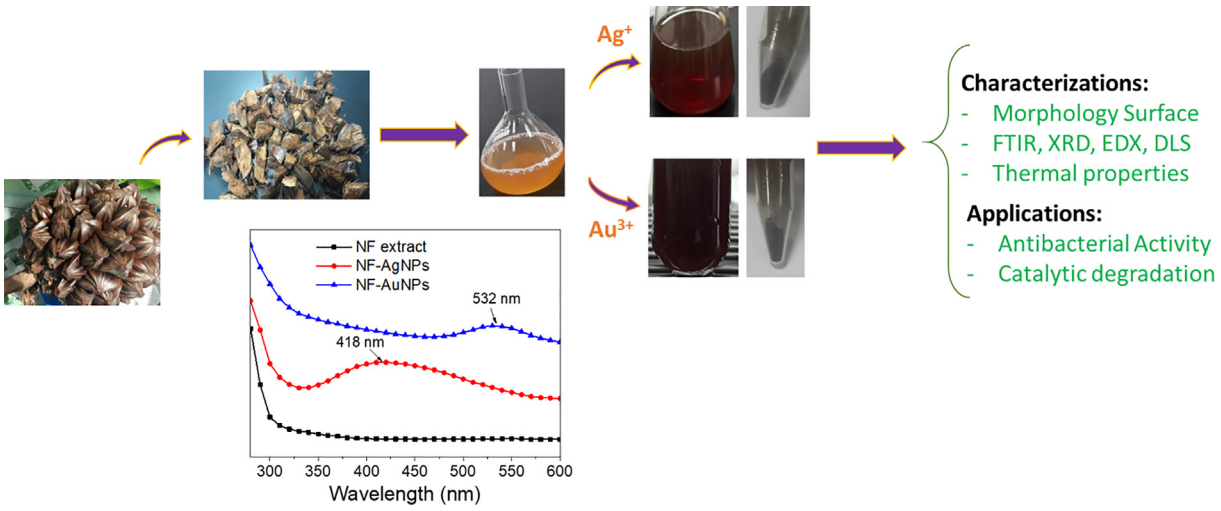

Fig. 2 Schematic illustration for study of NF-AgNPs and NF-AuNPs biosynthesized from waste *Nypa fruticans* fruit husk extract.

ence in size and morphology of MNPs can induce deviation in their activity. Thus, the biosynthesis process should be investigated parameters to find optimum reaction conditions (Nguyen et al. 2020). UV–Vis spectroscopy are used to determine the formation of the nanoparticles. NF-AgNPs and NF-AgNPs showed absorption peaks of surface plasmon resonance (SPR) at 418 nm and 532 nm, respectively while there is no absorption peak of the extract in range of 280–600 nm. The biosynthesized MNPs at optimized conditions are purified and followed physicochemical characterizations. The biogenic nanoparticles are applied for antibacterial assay and catalytic reduction of nitrophenols.

3.2. Optimization of reaction parameters

The change in reaction condition can affect the reducing ability of the bioactive molecules presented in the waste NF fruit husk extract. Hence, the formation of MNPs strongly depends on the reaction conditions. In this work, the effects of various factors such as the concentration of silver, reaction temperature and time on the biosynthesis were investigated. Fig. 3 shows absorbance spectra of NF-AgNPs dependent on the reaction parameters. The appearance of SPR peaks at low concentration of AgNPs (0.1 mM) indicated the formation of AgNPs. The increase of absorbance at the SPR bands along with gradually concentrated solutions around 0.1–10 mM is observed. The highest yield of the nanoparticles is obtained at Ag^+ concentration of 3.0 mM. For influence of reaction temperature, the reduction of NF-AgNPs was carried out in range of 30–90 °C and the formation yield of AgNPs is observed with increase of temperature (Fig. 3C and 3D). Intensive SPR peaks are not found at range of the low temperature (below 60 °C). At higher temperatures, the absorption peaks appear clearly and the absorbance values increase rapidly with growth of the temperature.

To study the effect of reaction time on the biosynthesis of NF-AgNPs, the mixture was stirred at 90 ^{0}C for 90 min and the reaction was monitored for each interval of 30 min. Upon the completing heating process, the appearance of absorption peaks is observed and the absorbance value is gradually increased over time which means the increasing yield of AgNPs.

The biosynthesis of NF-AuNPs also based on similar conditions of NF-AgNPs synthesis. The results show that the trend is observed differently from the biosynthesis of NF-AgNPs (Fig. 4). Regarding the effect of gold ion concentrations on the biosynthesis of AuNPs, there are no SPR peaks appeared at low concentration (< 0.5 mM) and high concentrations (> 1mM). A maximum absorbance was found at concentration of 0.5 mM. Great amount of gold precipitate was observed at range of high gold ion concentrations, explained the disappearance of SPR band. It can be because biomolecules presented in the extract are not enough to stabilize AuNPs generated from the reduction.

For study of reaction temperature, the reduction of AuNPs is easier in comparison with AgNPs formation. The SPR band at around 540 nm was appeared at range of low temperatures (even 25 °C). As seen in Fig. 4C, the effect of reaction temperature on the formation of AuNPs was not so significant. The increase of reaction temperature induces no change of absorbance values of the SPR band.

Fig. 4E & 4F showed that reduction of AuNPs induces slow increase of nanoparticles concentration in solution with reaction time. The conversation of AuNPs achieved a maximum value in 20 min.

For further studies on characterization and application, The MNPs were fabricated at optimized reaction conditions.

3.3. Characterizations

3.3.1. FTIR spectroscopy

FTIR spectroscopy was used to determine functional groups in the biosynthesized MNPs which acted as the capping agents in the extract during the synthesis. Fig. 5 showed the FTIR spectra of the NF extract and the final products of nanoparticles. Accordingly, spectra of the extract revealed major bands at 3417, 1620, 1520, 1444, 1377, 1257, 1144 cm^{-1}. The broad band at 3417 cm^{-1} relates to the OH stretching vibration of alcohol, phenolic, carbohydrate compounds and carboxylic acids. The sharp peak at 1630 cm^{-1} is assigned to C═C and

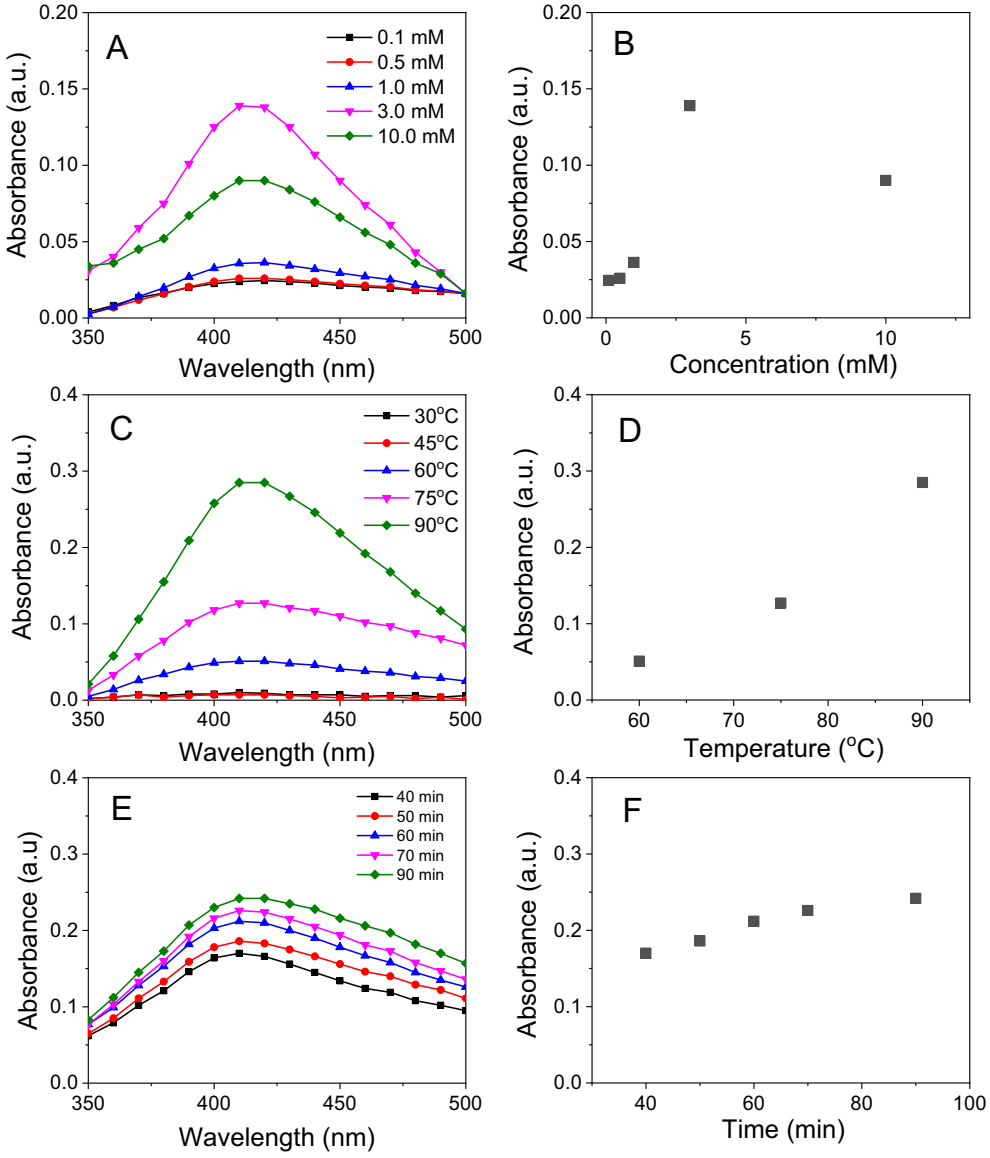

Fig. 3 UV–vis spectra (left) and plots of parameters versus absorbance (right) of NF-AgNPs: Concentration (A & B), reaction temperature (C & D) and reaction time (E & F).

C═O groups related to aromatic compounds and carbonyl group of protein molecules. The peak at 1377 cm^{-1} confirmed the presence of C─H group of carbohydrate compounds. The bands at 1257 cm^{-1} showed the in-plane bending vibration of OH groups of phenolic compounds (Odeniyi et al. 2020; Hamedi and Shojaosadati 2019; Adebayo-Tayo et al. 2019). Comparison of the FTIR spectra between the NF extract and the biosynthesized nanoparticles showed minor difference in the wavelength numbers as well as intensity of observed peaks. The spectra of NF-AgNPs and NF-AuNPs show corresponding wavenumbers at 3408, 1629, 1546, 1384, 1265, 1109 cm^{-1} and at 3188, 1610, 1515, 1438, 1278, 1103 cm^{-1}, respectively. These bands of the extract shifting new positions can relate to interactions between biomolecules and the MNPs. As a result, the biomolecules presented in the extract are proved as reducing and stabilizing agents during the biosynthesis of MNPs.

3.3.2. X-ray diffraction (XRD)

The crystalline nature and size of biosynthesized MNPs can be confirmed by the analysis of XRD patterns as shown in Fig. 6. The Bragg reflections of NF-AuNPs were observed at 2θ values 38.22°, 44.04°, 64.68°, and 77.36° which correspond to the face-centered cubic (FCC) planes of gold indexed as (111), (200), (220), and (311), respectively (card no. 00-004-0784). The XRD pattern of NF-AgNPs showed small peaks at 2θ values of 38.32°, 44.42°, 64.82° and 77.82° assigned to (111), (200), (220), and (311) FCC planes of AgNPs crystalline, respectively (card no. 00-004-0783). The strong peaks at 27.84°, 32.28°, 46.24°, 54.80°, 57.44° and 67.30° correspond to reflections from (111), (200), (220), (311), (222), and (420) planes of crystallite AgCl, respectively (card no. 00-001-1013) (Vo et al. 2019). The presence of AgCl crystalline in the NF-AgNPs can be due to the reaction of Ag^{+} ion with

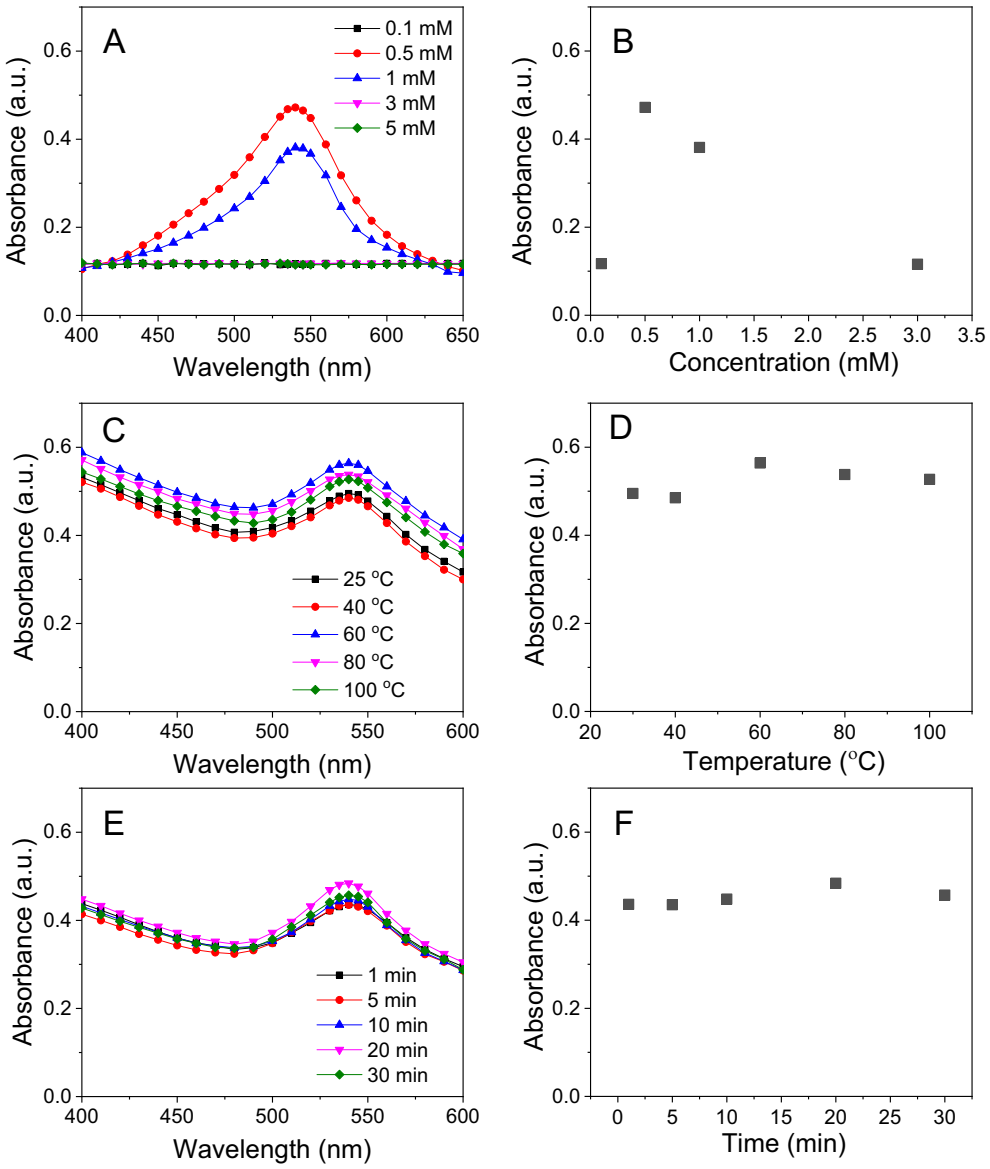

Fig. 4 UV–vis spectra (left) and plots of parameters versus absorbance (right) of NF-AuNPs: Concentration (A and B), reaction temperature (C and D) and reaction time (E and F).

chloride ion which presented with a high content in NF extract.

The XRD patterns can be used to determine the particle size by calculated from Debye-Scherrer equation $d = 0.9\lambda/\beta\cos\theta$, where 'd' is the average crystallite size in nm; 'θ' is the Bragg angle; 'λ' is the X-ray wavelength (0.1540 nm) and 'β' is the line broadening at half of the maximum intensity calculated by (π/180) × FWHM (full width at half maximum). Mean size of AuNPs calculated at (1 1 1) FCC plane of XRD pattern is estimated to be about 9.5 nm while mean size of AuNPs is calculated to be about 22.9 nm. The mean size of crystallite AgCl estimated from Debye-Scherrer's equation is 38.1 nm.

3.3.3. Morphology and elemental analysis

The surface morphologies and size of the synthesized AgNPs are determined by SEM and TEM analysis. The elemental composition presented in the samples is analyzed by EDX spectra represented the vertical axis with the number of X-ray counts and the horizontal axis with energy (keV). The results are shown in Figs. 7 and 8. The aqueous NF extract played a vital role in capping AgNPs can affect the morphology and elemental composition presented in the sample. The SEM image of biosynthesized AgNPs reveals that the spherical shapes dispersed non-uniformly and formed clusters (Fig. 7A). For EDX analysis, the strong elemental signal at 3.0 keV confirms the presence of silver in the sample. The presence of carbon and oxygen elements in the spectrum suggests that organic molecules of the NF extract were adsorbed on the surface of AgNPs. The appearance of chloride peak at 2.6 keV reveals the AgCl component which is in agreement of XRD data. The presence of other peaks such as 1.0, 2.1, 2.4 and 3.6 keV was assigned to elemental signals of Na, P, S, and K, respectively that presented in the aqueous extract of waste NF fruit

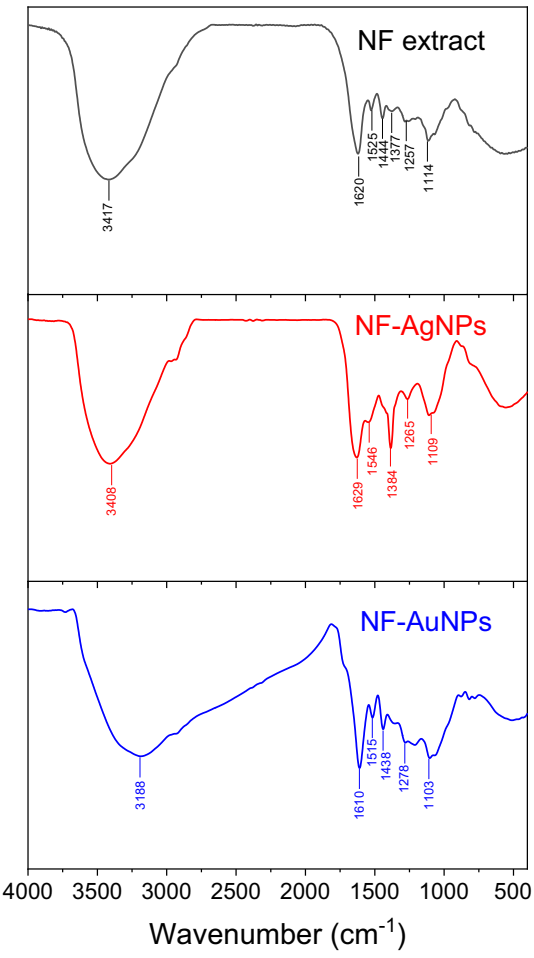

Fig. 5 FTIR spectra of NF fruit husk extract, NF-AgNPs and NF-AuNPs.

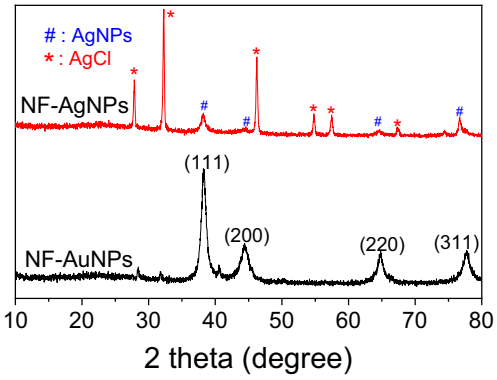

Fig. 6 XRD patterns of biosynthesized NF-AgNPs and NF-AuNPs.

husk. From EDX spectra data, average contents of elements in NF-AgNPs were plotted in Fig. 7C. Result shows that the sample contains about 26% (w/w) of silver and 13% (w/w) of chloride. The content of carbon which represents organic compounds in the sample is about 38% (w/w). TEM analysis is used to determine shape and size of metallic nanoparticles. Fig. 7D &7E shows the TEM images and the particle size distribution of NF-AgNPs. It is clear- that most of the nanoparticles are in spherical shape and well dispersed. The size of nanoparticles is distributed from 5 to 30 nm and mean particle size is found to be 10–15 nm. The HRTEM image of NF-AgNPs showed that the fringe spacing was 0.24 nm which correlated well with the spacing between (1 1 1) plane of FCC silver. The selected area of electron diffraction (SAED) pattern reveals bright rings, indicating the presence of crystalline nature. The bright circular rings correspond to reflection planes of AgNPs and AgCl as also observed in the previous report (Doan et al. 2020).

SEM images of biosynthesized AuNPs showed that the particles dispersed well on the surface (Fig. 8A). The EDX analysis appeared similar peaks in the patterns of NF-AgNPs (Fig. 8B & 8C). The strong peaks of potassium, chloride elements relating to their high contents (19% and 27% (w/w), respectively) in the sample were observed. The data showed three strong signals for gold at 2.1, 8.5 and 9.7 keV. A low content of gold in the samples was observed approx. 13%. Percentage of carbon (26.5%) is lower than that of the NF-AgNPs. It can be because NF-AuNPs contain different capping agents from NF-AgNPs. TEM images confirm that most of AuNPs exist in spherical shape and dispersed consistently. Their sizes are in range of 5–30 nm with a mean size of 15–20 nm (Fig. 8D & 8E). HRTEM images and SAED patterns clearly confirm crystal lattice nature of NF-AuNPs which are in agreement of XRD data (Fig. 8F). The lattice fringe corresponding to the (1 1 1) plane had spacing of 0.22 nm. The bright circular rings in SAED images relating to (1 1 1), (2 0 0), (2 2 0) and (3 1 1) Bragg's reflection planes of AuNPs indicated nanoparticles existed in crystalline nature.

3.4. Stability of colloidal solutions

Due to agglomeration of nanoparticles in colloidal solutions over time which strongly influence on the properties and applications, their stability in the solutions should be investigated. To study stability of nanoparticles, both colloidal solutions were exposed to daylight and measured UV–vis spectroscopy after various times after 3, 7, 14, 21 and 30 days. Stability of the colloidal solutions can be determined by decrease of absorbance values at the SPR band in UV–Vis spectra. As shown in Fig. 9, both the nanoparticles began to slightly agglomerate in initial 3 days. Decrease of the nanoparticle concentration (about 7–8%) in the colloidal solutions was estimated. Rapid decrease in stability of the solutions is observed according to the investigated time. Stability of the nanoparticle solutions was around 70–77% after 14 days of the exposition and remained around 35–46% after 30 days of the exposition. The NF-AgNPs solution possessed a slightly higher stability in comparison with NF-AuNPs.

3.5. Antibacterial assay

Antibacterial activity of both the biosynthesized nanoparticles was tested against three strains including *B. cereus, S. aureus* (Gram-positive) and *S. typhimurium* (Gram-negative) with various concentrations. The extract and ampicillin were used as the negative and positive controls, respectively. The results showed that NF-AuNPs did not exhibit bioactivity

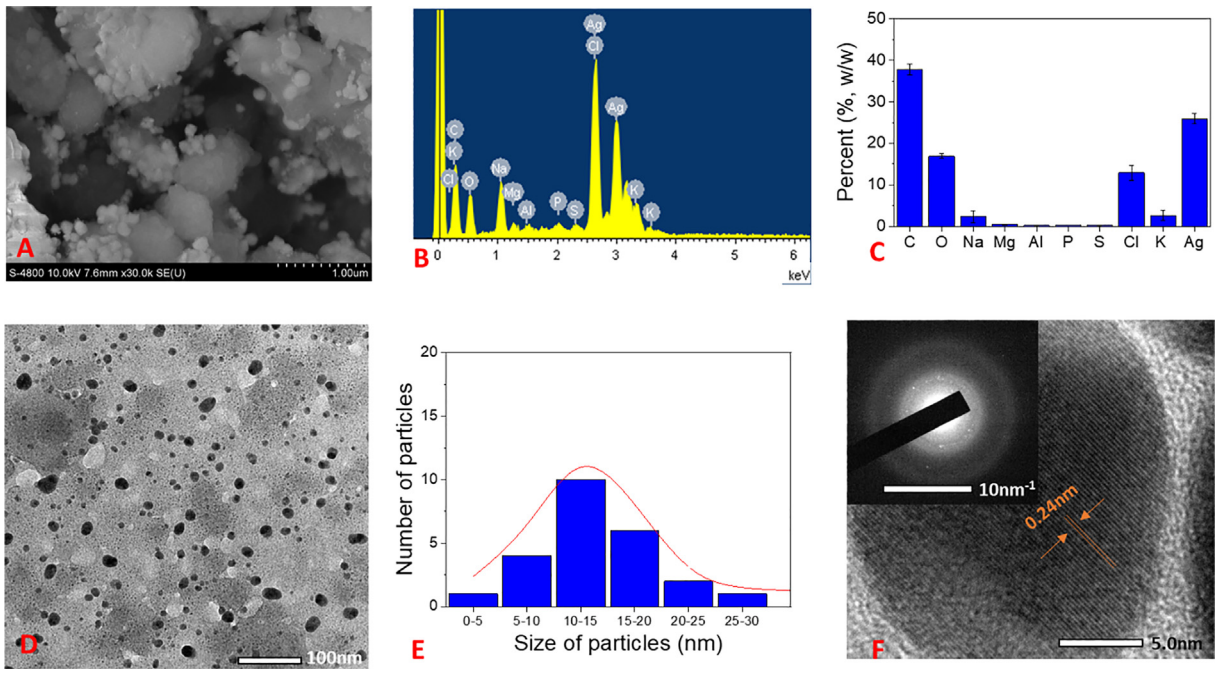

Fig. 7 (A) SEM image; (B) EDX spectrum; (C) Elemental percent collected from EDX spectrum; (D) TEM and SAED pattern (inset); (E) particle size distribution; and (F) HRTEM of NF-AgNPs.

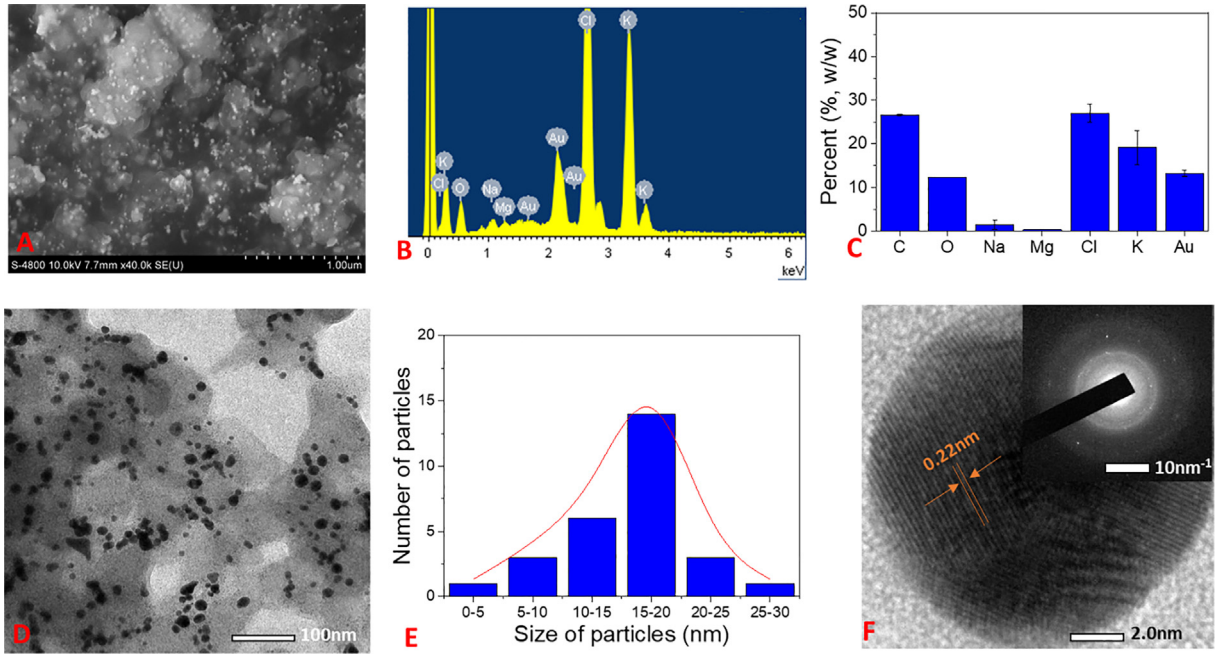

Fig. 8 (A) SEM image; (B) EDX spectrum; (C) Elemental percent collected from EDX spectrum; (D) TEM and SAED pattern (inset); (E) particle size distribution; and (F) HRTEM of NF-AuNPs.

against any bacterial strain even at the highest concentration (8.95 μg/mL) while the sample of NF-AgNPs exhibited selective antibacterial activity against three tested strains. The results of antibacterial activity for the NF-AgNPs are listed in Table 1. The antibacterial effect of NF-AgNPs was presented in zone of inhibition and influence of concentrations on their bioactivity was investigated. The results showed that the sample NF-AgNPs exhibited high antibacterial activity against *B. cereus* but it did not inhibit two strains, *S. aureus* and *S. typhimurium* at tested concentration. Moreover, the bioactivity is increasing with increase of the biosynthesized NF-AgNPs concentration. The minimum inhibitory concentration (MIC) value of NF-AgNPs against *B. cereus* was found to be 1.24 μg/mL.

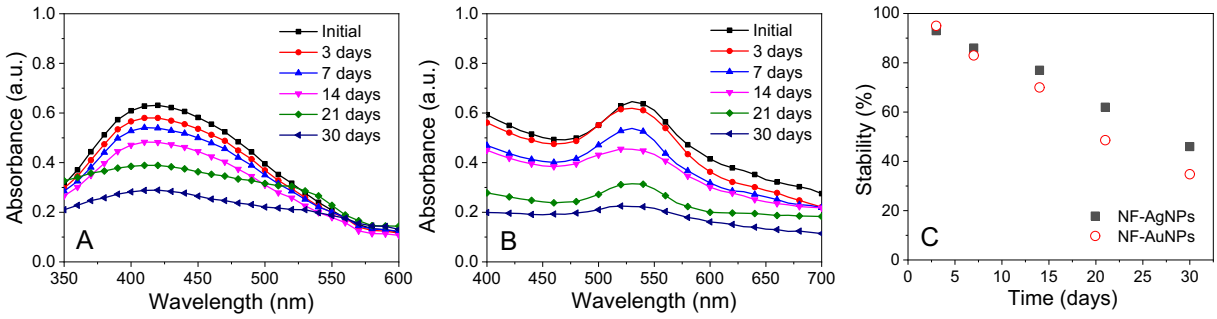

Fig. 9 UV–Vis spectra of NF-AgNPs (A) and NF-AuNPs (B) and plot of stability against time (C).

Table 1 Antibacterial effect of NF-AgNPs at various concentrations.

Bacterial strains	Zone of inhibition (mm)					
	Ampicillin	Extract	Concentration of NF-AgNPs (μg/mL)			
			0.62	1.24	2.48	4.96
B. cereus	18.5	6	6	7	9	12
S. aureus	24	6	6	6	6	6
S. typhimurium	26	6	6	6	6	6

3.6. Catalytic performance for reduction of nitrophenols

Organic aromatic substances especially nitrophenols, which are extensively used in industrial process, possess highly toxic effects in aquatic environment. The presence of low concentration of nitrophenols also poses serious threat to the life environment because it is difficult to degrade in the normal condition (Gul et al. 2017; Albukhari et al. 2019). Moreover, catalytic hydrogenation of nitrophenols into aminophenols has potential of great pharmaceutical application. The aminophenols are essential precursors for synthesis of numerous drugs such as paracetamol and phenacetin (Majumdar et al. 2016). In the present work, evaluation of catalytic performance for reduction of *o*-, *m*-, *p*-nitrophenols in aqueous medium was performed by catalytic hydrogenation of $NaBH_4$ using UV–vis method as a model reaction. It is well known that reduction of nitrophenols using $NaBH_4$ without catalyst is a thermodynamically favorable reaction but it is also a kinetically unfavorable reaction due to the kinetic barrier between the BH_4^- and nitrophenolate ions. In fact, intensity and maximum peaks of nitrophenols in UV–vis spectra remain unchanged over time without the catalyst as reported elsewhere (Vo et al. 2020; Nguyen et al. 2019a,b). This barrier can be overcome by the addition of catalyst such as noble metals that performed via an electron transfer mechanism. In this mechanism, both borohydride and nitrophenolate ions are played roles as donor and acceptor, adsorbed/released on the catalyst surface where electrons are transferred from borohydride to nitrophenolate ion (Nguyen et al. 2019a,b). Therefore, the catalytic effect is dependent on the property of both reagents and catalyst. Moreover, the reusability of noble metal catalysts is particularly necessary to effectively reduce the cost.

Results for the remediation of nitrophenols in the presence of the biosynthesized AgNPs are shown in Fig. 10. The absorption spectra of the reactions were directly tested from the cuvette. With the addition of $NaBH_4$, the color change was observed for all nitrophenols and the maximum peaks of *o*-, *m*- and *p*-nitrophenols shifted to new positions at 415, 391 and 400 nm, respectively. The regular decline of the corresponding peaks and formation of aminophenols with increasing absorbance of new peaks were observed upon completing addition of the catalyst. Due to high amount of $NaBH_4$ (excess 200 times) and very little amount of the nanoparticles (3 mg), the kinetic of nitrophenols reduction follows the pseudo first order reaction (Nguyen et al. 2020). The recyclable performance of the catalysts was also tested for five reaction recycles. The catalyst was washed with distilled water and then ethanol before each reuse process performed.

Fig. 10 shows that reduction time of all nitrophenols using NF-AgNPs was completed in 9 min while the rate constants of the nitrophenols were slightly different. The rate constant values of *o*-, *m*- and *p*-nitrophenols were found to be $3.54x10^{-3}$, $2.49x10^{-3}$ and $2.70x10^{-3}s^{-1}$, respectively. The recycling process showed that the recycle ability of NF-AgNPs is strongly dependent on the substrate structure. The catalysis performance of NF-AgNPs was stable in the reduction of *o*- and *p*-nitrophenols without decays after 5 successive recycles (yield > 97%) whereas yield of *m*-nitrophenol reduction reduced to 80% after the first recycle. It can be because adsorbed or/and released process of *m*-nitrophenol is slower than the other substrates. However, trend of the nitrophenol reduction in the presence of AgNPs was not unique with the previous study (Doan et al. 2020). It can relate to difference of chemical compositions, especially content of AgCl between the catalysts. Although composite Ag@AgCl is well known as an effective catalyst for the reduction of nitrophenols (Konvičková et al. 2018; Attia and Mohamed, 2018; Zhou et al. 2017), the role of AgCl in this reaction has not been eval-

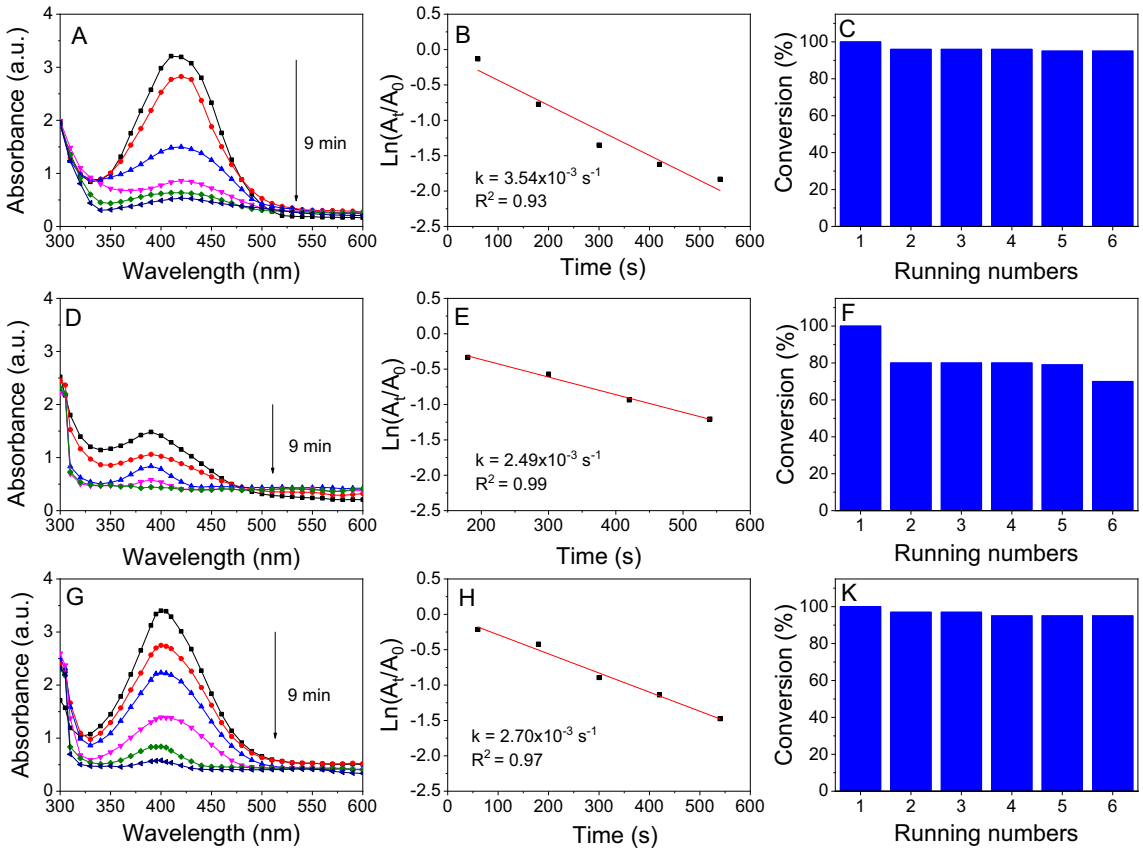

Fig. 10 UV–vis spectra (left), first order kinetics (middle) and conversion efficiency for 5 running numbers (right) of *o*-nitrophenol (A, B, C), *m*-nitrophenol (D, E, F) and *p*-nitrophenol (G, H, I) by $NaBH_4$ in the presence of NF-AgNPs.

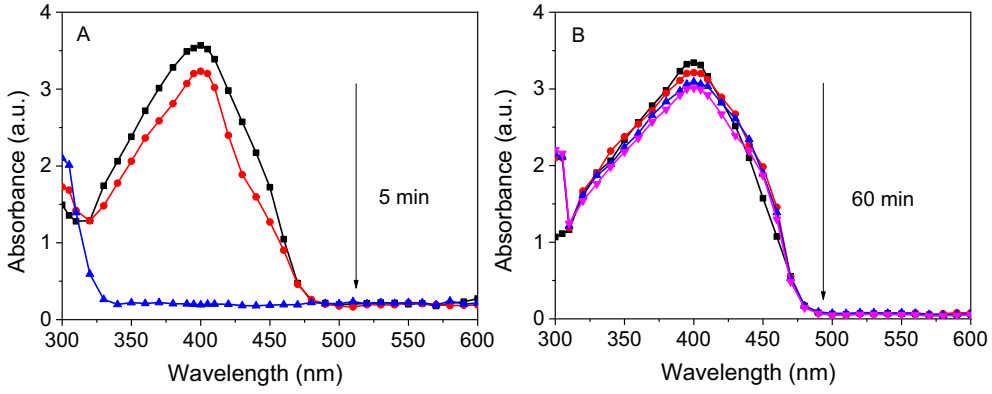

Fig. 11 UV–vis spectra of reduction of *p*-nitrophenol by $NaBH_4$ in the presence of AgCl (A) and reused AgCl (B).

uated. In the present work, we investigated the reduction of 4-nitrophenol in the presence of crystalline AgCl catalyst and its recyclable ability.

The reaction was carried out under the same conditions with the presence of crystalline AgCl and recognized by progressive decrease of the absorbance at 400 nm in UV–vis spectra. The results revealed that the crystalline AgCl was an effective catalyst and the reaction was rapidly completed in only 5 min (Fig. 11A). For the recycle process, the catalyst sample was washed with water and ethanol to remove organic compounds before reuse. Fig. 11B showed that the absorbance values almost were not decreased in 60 min after addition of the catalyst, indicating the crystalline AgCl deactivated after the first recycle. Therefore, it is supposed that surface of crystalline AgCl is attached by the other molecules which can induce deactivation of the catalyst. To study chemical compositions, the used catalyst was measured XRD spectroscopy. The result shows the XRD pattern of the used catalyst appeared peaks at 2θ values of crystallite silver similarly to that of the NF-AgNPs sample (Fig. 12). It revealed that the used catalyst was covered by the crystalline silver which could be formed from the reduction of AgCl molecules into crys-

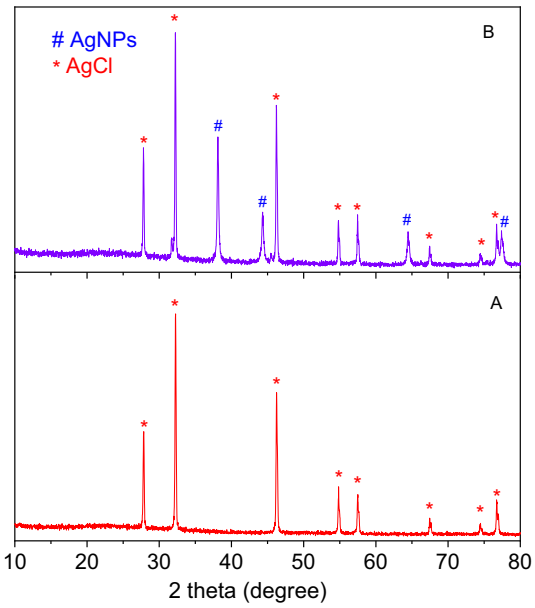

Fig. 12 XRD pattern of AgCl before reduction of *p*-nitrophenol (A) and after reduction of *p*-nitrophenol (B).

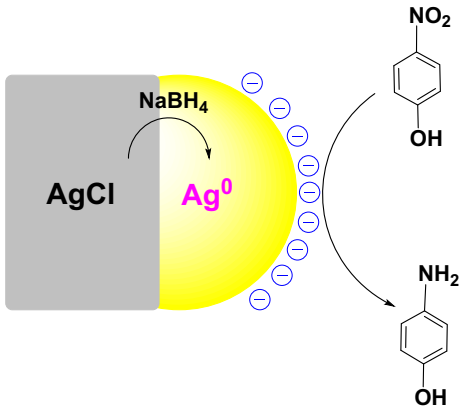

Fig. 13 Proposed mechanism of AgCl catalyst for reduction of *p*-nitrophenol.

talline silver on their surface by $NaBH_4$. As a result, the established crystalline silver played a role as an effective catalyst for reduction of *p*-nitrophenol. Due to the disappearance of surfactants, the crystalline silver with large size, which is approved by sharply intense peaks in the XRD pattern, covers on the AgCl surface led to a low surface area of the catalyst. Thus, the crystalline AgCl is easy to be deactivated in the first recycle. A proposed mechanism of the AgCl catalyst can be illustrated in Fig. 13. It reveals the role of AgCl in NF-AgNPs sample as a source supplying AgNPs in the catalytic reduction of *p*-nitrophenol using $NaBH_4$.

For the catalytic reduction of nitrophenols in the presence of NF-AuNPs, the results are shown in Fig. 14. A different trend was observed in comparison with the NF-AgNPs catalyst. The significant decrease of catalytic performance for hydrogenation of *o*-nitrophenol and *m*-nitrophenol can be confirmed by increase of reaction time (15 min) while the performance of *p*-nitrophenol hydrogenation is increasing with reduction of reaction time (5 min). The rate constants of NF-AuNPs catalyst for reduction of *o*-nitrophenol, *m*-nitrophenol and *p*-nitrophenol were found to be 2.34×10^{-3} s^{-1}, 1.12×10^{-3} s^{-1} and 3.42×10^{-3} s^{-1}, respectively. It clearly reveals that the catalytic reduction of nitrophenols is dependent on both the nanoparticles and reactants due to different interaction of nitrophenols and nanoparticle surfaces (Doan et al. 2020). A comparison of catalysis activity with previous reports is shown in Table S1. For recycling process, it is observed that the recyclable ability of NF-AuNPs is lower than that of NF-AgNPs. The hydrogenation performance of *o*-nitrophenol is gradually declined after six running numbers and achieved 80% at the sixth run while yield of *m*-nitrophenol reduction decreased (about 82%) after the second run. The stability of NF-AuNPs catalyst for *p*-nitrophenol reduction is very much lower than stability of NF-AgNPs. Catalytic yield of NF-AuNPs reduced to 68% after the second run.

In addition to rate constant, turnover number (TON) and the turnover frequency (TOF) are important parameters used for comparison of catalyst performance. In this heterogeneous catalyst, TON is the number of nitrophenol moles that 1 mol of nanocatalyst may convert into aminophenol. TOF value is simply calculated by TON/time. For NF-AgNPs catalyst, TOF values for three nitrophenols were found to be 6.4×10^{-5} s^{-1} while higher values were found for NF-AuNPs catalyst. TOF values are calculated to be 2.1×10^{-4} s^{-1} for *o*- and *m*-nitrophenol reductions and 6.3×10^{-4} s^{-1} for *p*-nitrophenol reduction in NF-AuNPs catalyst. The high TOF values of NF-AuNPs catalyst are attributed to a low content of gold in NF-AuNPs catalyst compared with that of silver in NF-AgNPs catalyst although reaction time of NF-AuNPs catalyst is higher.

4. Conclusions

In this study, highly efficient and simple synthesis of noble metal nanoparticles was accomplished by utilization of waste *Nypa fruticans* fruit husk extract. This method not only offered a low-cost and reduced-toxic synthesis but also used effectively the waste sources in the agricultural field. The biomolecules in the aqueous extract acted as capping agent and reducing agent allowed a transformation of metallic ions to MNPs. The cations and anions presented in the extract was major reasons to explain presence of AgCl in the NF-AgNPs and low content of metallic nanoparticles in the solid samples. Average size of AgNPs and AuNPs is about 10–15 nm and 15–20 nm, respectively. NF-AgNPs exhibited selective antibacterial activity that showed the strong bioactivity against *B. cereus* but no activity against *S. aureus* and *S. typhimurium* at all tested concentrations. The biosynthesized nanoparticles also demonstrated potentially recyclable catalysts in reduction of nitrophenols into the corresponding aminophenols. The presence of AgCl in NF-AgNPs as a source supplying AgNPs for the reduction reaction. The kinetic studies showed that rate constants of NF-AgNPs were higher than those of NF-AuNPs. However, TOF values of NF-AuNPs were found to be greater than those of NF-AgNPs. The nanoparticles could be used effectively with six running numbers. Hence, the noble nanoparticles biosynthesized from this waste source encompass a wide range of applications that can be used for varied scientific domains.

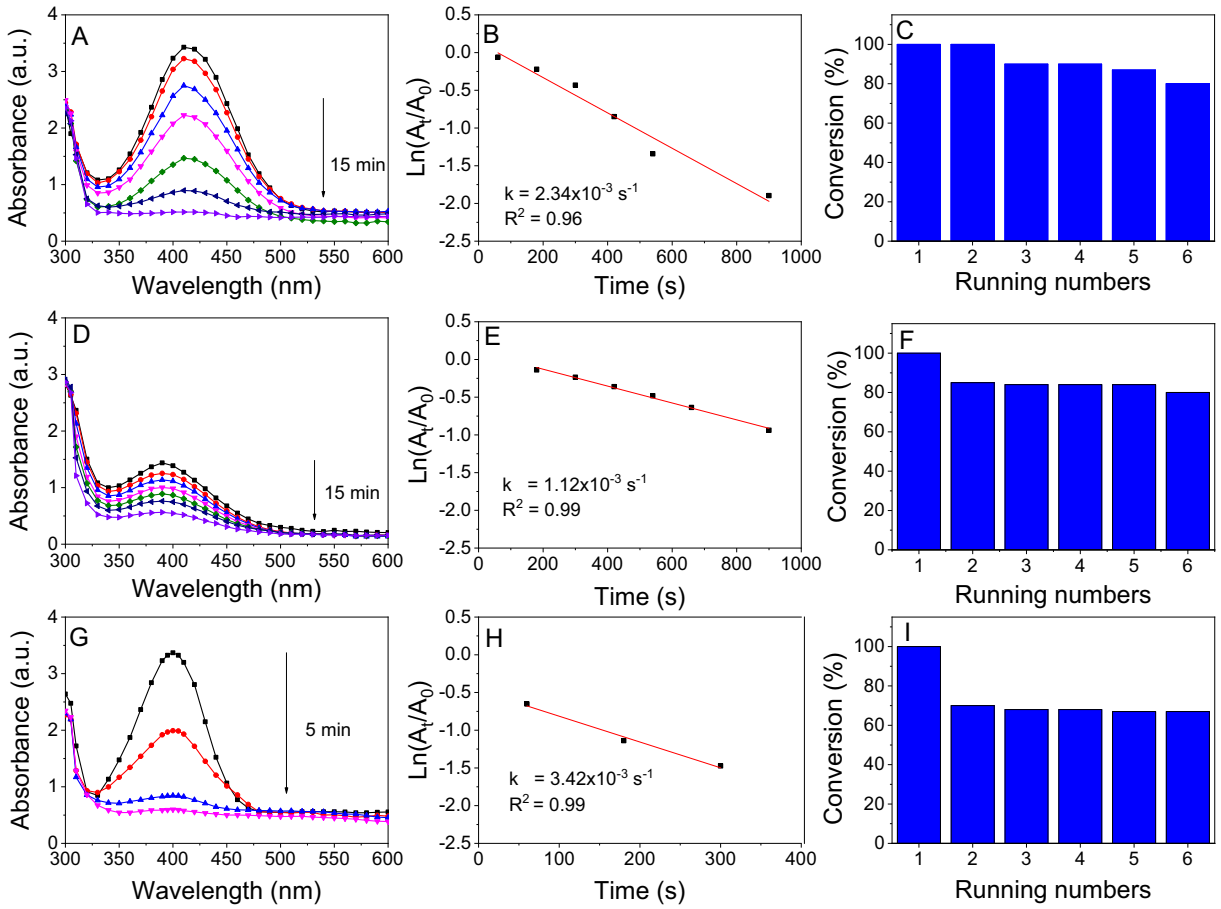

Fig. 14 UV–vis spectra (left), first order kinetics (middle) and conversion efficiency for 6 running numbers (right) of *o*-nitrophenol (A, B, C), *m*-nitrophenol (D, E, F) and *p*-nitrophenol (G, H, I) by $NaBH_4$ in the presence of NF-AuNPs.

Declaration of Competing Interest

No potential conflict of interest was reported by the authors.

Appendix A. Supplementary material

Supplementary data to this article can be found online at https://doi.org/10.1016/j.arabjc.2020.08.024.

References

Abdelghany, T.M., Al-Rajhi, A.M.H., Abboud, M.A.A., Alawlaqi, M. M., Magdah, A.G., Helmy, E.A.M., Mabrouk, A.S., 2018. Recent advances in green synthesis of silver nanoparticles and their applications: about future directions. A review. BioNanoScience 8, 5–16.

Adebayo-Tayo, B., Salaam, A., Ajibade, A., 2019. Green synthesis of silver nanoparticle using Oscillatoria sp. extract, its antibacterial, antibiofilm potential and cytotoxicity activity. Heliyon 5, e02502.

Agnihotri, S., Sillu, D., Sharma, G., Arya, R.K., 2018. Photocatalytic and antibacterial potential of silver nanoparticles derived from pineapple waste: process optimization and modeling kinetics for dye removal. Appl. Nanosci. 8, 2077–2092.

Albukhari, S.M., Ismail, M., Akhtar, K., Danish, E.Y., 2019. Catalytic reduction of nitrophenols and dyes using silver nanoparticles @ cellulose polymer paper for the resolution of waste water treatment challenges. Colloids Surf A: Physicochem. Eng. Aspects 577, 548–561.

Attia, Y.A., Mohamed, Y.M.A., 2018. Silicon-grafted Ag/AgX/rGO nanomaterials (X = Cl or Br) as dip-photocatalysts for highly efficient p-nitrophenol reduction and paracetamol production. Appl. Organometal. Chem. 33, e4757.

Burlacu, E., Tanase, C., Coman, N.A., Berta, L., 2019. A Review of bark-extract-mediated green synthesis of metallic nanoparticles and their applications. Molecules 24, 4354.

Darabdhara, G., DasSurya, M.R., Aravind, P.S., Sabine, K.R., Boukherroub, S.R., 2019. Ag and Au nanoparticles/reduced graphene oxide composite materials: Synthesis and application in diagnostics and therapeutics. Adv. Colloid Interface Sci. 271, 101991.

Das, S., Chakraborty, J., Chatterjee, S., Kumar, H., 2018. Prospects of biosynthesized nanomaterials for the remediation of organic and inorganic environmental contaminants. Environ. Sci. Nano 5, 2784–2808.

Doan, V.D., Luc, V.S., Nguyen, T.L.H., Nguyen, T.D., Nguyen, T.D., 2020. Utilizing waste corn-cob in biosynthesis of noble metallic nanoparticles for antibacterial effect and catalytic degradation of contaminants. Environ. Sci. Pollut. Res. 27, 6148–6162.

Dodevska, T., Vasileva, I., Denev, P., Karashanova, D., Georgieva, B., Kovacheva, D., Yantcheva, N., Slavov, A., 2019. *Rosa damascena* waste mediated synthesis of silver nanoparticles: Characteristics and application for an electrochemical sensing of hydrogen peroxide and vanillin. Mater. Chemis. Phys. 231, 335–343.

Fagherazzi, S., Bryan, K.R., Nardin, W., 2017. Buried alive or washed away: The challenging life of mangroves in the Mekong Delta. Oceanography 30, 48–59.

Francis, S., Joseph, S., Koshy, E.P., Mathew, B., 2017. Synthesis and characterization of multifunctional gold and silver nanoparticles using leaf extract of *Naregamia alata* and their applications in the catalysis and control of mastitis. New J. Chem. 41, 14288–14298.

Ghasemi, Z., Abdi, V., Sourinejad, I., 2020. Single-step biosynthesis of Ag/AgCl@TiO2 plasmonic nanocomposite with enhanced visible light photoactivity through aqueous leaf extract of a mangrove tree. Appl. Nanosci. 10, 507–516.

Gul, S., Rehan, Z.A., Khan, S.A., Akhtar, K., Khan, M.A., Khan, M. I., Rashid, M.I., Asiri, A.M., Khan, S.B., 2017. Antibacterial PES-CA-Ag_2O nanocomposite supported Cu nanoparticles membrane toward ultrafiltration, BSA rejection and reduction of nitrophenol. J. Mol. Liq. 230, 616–624.

Hamedi, S., Shojaosadati, S.A., 2019. Rapid and green synthesis of silver nanoparticles using Diospyros lotus extract: Evaluation of their biological and catalytic activities. Polyhedron 171, 172–180.

Hamilton, L.S., Murphy, D.H., 1988. Use and management of nipa palm (*Nypa fruticans*, Arecaceae): a review. Econ. Bot. 42, 206–213.

Hui, Y., Zhang, S., Wang, W., 2019. Recent progress in catalytic oxidative transformations of alcohols by supported gold nanoparticles. Adv. Synth. Catal. 361, 2215–2235.

Jamila, N., Khan, N., Bibi, A., Haider, A., Khan, S.N., Atlas, A., Nishan, U., Minhaz, A., Javed, F., Bibi, A., 2020. *Piper longum* catkin extract mediated synthesis of Ag, Cu, and Ni nanoparticles and their applications as biological and environmental remediation agents. Arab. J. Chem. 13, 6425–6436.

Kalantari, K., Afifi, A.B.M., Bayat, S., Shameli, K., Yousefi, S., Mokhtar, N., Kalantari, A., 2019. Heterogeneous catalysis in 4-nitrophenol degradation and antioxidant activities of silver nanoparticles embedded in Tapioca starch. Arab. J. Chem. 12 (8), 5246–5252.

Khan, F., Iqbal, S., Khalid, N., Hussain, I., Hussain, Z., Szmigielski, Z., Janjua, H.A., 2020. Screening and stability testing of commercially applicable Heliotropium crispum silver nanoparticle formulation with control over aging and biostability. Appl. Nanosci. 10, 1941–1956.

Khan, S., Runguo, W., Tahir, K., Jichuan, Z., Zhang, L., 2017. Catalytic reduction of 4-nitrophenol and photo inhibition of *Pseudomonas aeruginosa* using gold nanoparticles as photocatalyst. J. Photochem. Photobiol. B Biol. 170, 181–187.

Konvičková, Z., Holišová, V., Kolenčík, M., Niide, T., Kratošová, G., Umetsu, M., Seidlerová, J., 2018. Phytosynthesis of colloidal Ag-AgCl nanoparticles mediated by Tilia sp. leachate, evaluation of their behaviour in liquid phase and catalytic properties. Colloid Polym. Sci. 296, 677–687.

Ly, N.H., Joo, S.W., 2020. Recent advances in cancer bioimaging using a rationally designed Raman reporter in combination with plasmonic gold. J. Mater. Chem. B 8, 186–198.

Majumdar, R., Bag, B.G., Ghosh, P., 2016. *Mimusops elengi* bark extract mediated green synthesis of gold nanoparticles and study of its catalytic activity. Appl. Nanosci. 6, 521–528.

Mosaviniya, M., Kikhavani, T., Tanzifi, M., Yaraki, M.T., Tajbakhsh, P., Lajevardi, A., 2019. Facile green synthesis of silver nanoparticles using *Crocus Haussknechtii Bois* bulb extract: Catalytic activity and antibacterial properties. Colloid Interface Sci. Com. 33, 100211.

Nam, N.N., Bui, T.L., Son, S.J., Joo, S.W., 2020. Ultrasonication-Induced Self-Assembled Fixed Nanogap Arrays of Monomeric Plasmonic Nanoparticles inside Nanopores. Adv. Funct. Mater. 29 (12), 1809146.

Nasrollahzadeh, M., Yek, S.M.G., Motahharifar, N., Gorab, M.G., 2019. Recent developments in the plant-mediated green synthesis of Ag-based nanoparticles for environmental and catalytic applications. Chemm. Rec. 19, 2436–2479.

Nguyen, T.D., Dang, V.S., Nguyen, V.H., Nguyen, T.M.T., Dang, C. H., 2018a. Synthesis and photophysical characterization of several 2,3-quinoxaline derivatives. An application of Pd(0)/PEG nanoparticle catalyst for Sonogashira coupling. Polycycl. Aromat. Comp. 38, 42–50.

Nguyen, T.M.T., Huynh, T.T.T., Dang, C.H., Mai, D.T., Nguyen, T. T.N., Nguyen, D.T., Dang, V.S., Nguyen, T.D., Nguyen, T.D., 2020. Novel biogenic silver nanoparticles used for antibacterial effect and catalytic degradation of contaminants. Res. Chem. Intermediates 46, 1975–1990.

Nguyen, T.D., Dang, C.H., Mai, D.T., 2018b. Biosynthesized AgNP capped on novel nanocomposite 2-hydroxypropyl-β-cyclodextrin/alginate as a catalyst for degradation of pollutants. Carbohyd. Polym. 197, 29–37.

Nguyen, T.D., Vo, T.T., Nguyen, C.H., Doan, V.D., Dang, C.H., 2019a. Biogenic palladium nanoclusters supported on hybrid nanocomposite 2-hydroxypropyl-β-cyclodextrin/alginate as a recyclable catalyst in aqueous medium. J. Mol. Liq. 276, 927–935.

Nguyen, T.D., Vo, T.T., Huynh, T.T.T., Nguyen, C.H., Doan, V.D., Nguyen, D.T., Nguyen, T.D., Dang, C.H., 2019b. Effect of capping methods on the morphology of silver nanoparticles: study on the media-induced release of silver from the nanocomposite β-cyclodextrin/alginate. New J. Chem. 43, 16841–16852.

Odeniyi, M.A., Okumah, V.C., Adebayo-Tayo, B.C., Odeniyi, O.A., 2020. Green synthesis and cream formulations of silver nanoparticles of Nauclea latifolia (African peach) fruit extracts and evaluation of antimicrobial and antioxidant activities. Sustain. Chem. Pharm. 15, 100197.

Phetrit, R., Chaijan, M., Sorapukdee, S., Panpipat, W., 2020. Characterization of Nipa Palm's (*Nypa fruticans* Wurmb.) Sap and Syrup as Functional Food Ingredients. Sugar Tech. 22, 191–201.

Rafique, M., Sadaf, I., Rafique, M.S., Tahir, M.B., 2017. A review on green synthesis of silver nanoparticles and their applications. Artif. Cells Nanomed. Biotechnol. 45, 1272–1291.

Sharma, D., Kanchi, S., Bisetty, K., 2019. Biogenic synthesis of nanoparticles: A review. Arab. J. Chem. 12, 3576–3600.

Singhal, A., Gupta, A., 2018. Efficient utilization of Sal deoiled seed cake (DOC) as reducing agent in synthesis of silver nanoparticles: Application in treatment of dye containing wastewater and harnessing reusability potential for cost-effectiveness. J. Mol. Liq. 268, 691–699.

Song, C., Ye, F., Liu, S., Li, F., Huang, Y., Ji, R., Li, Z., 2019. Thorough utilization of rice husk: metabolite extracts for silver nanocomposite biosynthesis and residues for silica nanomaterials fabrication. New J. Chem. 43, 9201–9209.

Tamunaidu, P., Saka, S., 2011. Chemical characterization of various parts of nipa palm (*Nypa fruticans*). Ind. Crops Prod. 34, 1423–1428.

Uhl, N.W., 1972. Inflorescence and flower structure in *Nypa fruticans* (Palmae). Am. J. Bot. 59, 729–743.

Veisi, H., Azizi, S., Mohammadi, P., 2018. Green synthesis of the silver nanoparticles mediated by *Thym braspicata* extract and its application as a heterogeneous and recyclable nanocatalyst for catalytic reduction of a variety of dyes in water. J. Clean Prod. 170, 1536–1543.

Vetchinkina, E., Loshchinina, E., Kupryashina, M., Burov, A., Nikitina, V., 2019. Shape and Size Diversity of Gold, Silver, Selenium, and Silica Nanoparticles Prepared by Green Synthesis Using Fungi and Bacteria. Ind. Eng. Chem. Res. 58, 17207–17218.

Vinay, S.P., Udayabhanu, Nagaraju, G., Chandrappa, C.P., Chandrasekhar, N., 2020. A novel, green, rapid, nonchemical route hydrothermal assisted biosynthesis of Ag nanomaterial by blush-wood berry extract and evaluation of its diverse applications. Appl. Sci. https://doi.org/10.1007/s13204-020-01289-y.

Vishwasrao, C., Momin, B., Ananthanarayan, L., 2019. Green Synthesis of Silver Nanoparticles Using Sapota Fruit Waste and

Evaluation of Their Antimicrobial Activity. Waste Biomass Valori. 10, 2353–2363.

Vo, T.T., Nguyen, T.T.N., Huynh, T.T.T., Vo, T.T.T., Nguyen, T.T. N., Nguyen, D.T., Dang, V.S., Dang, C.H., Nguyen, T.D., 2019. Biosynthesis of silver and gold nanoparticles using aqueous extract of *Crinum latifolium* leaf and their applications towards antibacterial effect and wastewater treatment. J. Nanomater. 2019, 8385935.

Vo, T.T., Dang, C.H., Doan, V.D., Dang, V.S., Nguyen, T.D., 2020. Biogenic synthesis of silver and gold nanoparticles from *Lactuca indica* leaf extract and their application in catalytic degradation of toxic compounds. J. Inorg. Organomet. Polym. Mater. 30, 388–399.

Wang, F., Zhang, W., Tan, X., Wang, Z., Li, Y., Li, W., 2019. Extract of *Ginkgo biloba* leaves mediated biosynthesis of catalytically active and recyclable silver nanoparticles. Colloids Surf. A: Physicochem. Eng. Aspects 563, 31–36.

Zhou, H., Che, L., Guo, X., Wang, X., Zhan, J., Wu, M., Hu, Y., Yi, X., Zhang, X., Liu, L., 2017. Interface modulation of bacteriogenic Ag/AgCl nanoparticles by boosting the catalytic activity for reduction reactions using Co^{2+} ions. Chem. Commun. 53, 4946–4949.

Zhu, G., Geng, J., Yan, L., Yuan, Y.K., Han, G.Z., 2019. Homogeneous magnetic Ag-Au alloy microparticles for ultrasensitive catalytic reduction of aromatic nitro compounds. Colloids Surf. A: Physicochem. Eng. Aspects 580, 123697.